

Self-similar collapse and the structure of dark matter halos: A fluid approach

Kandaswamy Subramanian

National Centre for Radio Astrophysics, Tata Institute of Fundamental Research, Poona
University Campus, Ganeshkhind, Pune 411 007, India.

ABSTRACT

We explore the dynamical restrictions on the structure of dark matter halos through a study of cosmological self-similar gravitational collapse solutions. A fluid approach to the collisionless dynamics of dark matter is developed and the resulting closed set of moment equations are solved numerically including the effect of halo velocity dispersions (both radial and tangential), for a range of spherically averaged initial density profiles. Our results highlight the importance of tangential velocity dispersions to obtain density profiles shallower than $1/r^2$ in the core regions, and for retaining a memory of the initial density profile, in self-similar collapse. For an isotropic core velocity dispersion only a partial memory of the initial density profile is retained. If tangential velocity dispersions in the core are constrained to be less than the radial dispersion, a cuspy core density profile shallower than $1/r$ cannot obtain, in self-similar collapse.

Subject headings: Cosmology: dark matter, Large-scale structure of Universe; Galaxies: Formation, Halos, clusters

1. Introduction

In hierarchical clustering theories of structure formation, like the cold dark matter (CDM) models, small mass clumps of dark matter form first and gather into larger and larger masses subsequently. The structure of these dark matter "halos", is likely to be related to how the halos formed, the initial spectrum of the density fluctuations and to the underlying cosmology. Several properties of galactic and cluster halos can be well constrained by observations. So, if the matter distribution in dark halos are fossils which do depend on some of the properties of structure formation models, like their initial power spectrum, one would have a useful observational handle on these properties. It is therefore necessary to understand what determines the matter distribution (or density profiles) of dark matter halos *ab initio*. This forms the motivation of the present paper and the companion paper by Subramanian, Cen and Ostriker (SCO99, 1999).

Further, Navarro, Frenk and White (NFW) (1995, 96, 97) have proposed from their N-body simulations, that dark matter halos in hierarchical clustering scenarios develop a universal density

profile, regardless of the scenario for structure formation or cosmology. The NFW profile has an inner cuspy form with the density $\rho \propto r^{-1}$ and an outer envelope of the form $\rho \propto r^{-3}$. Several investigators have found that the NFW profile provides a moderately good fit to numerical simulations (Cole and Lacey 1996, Tormen, Bouchet & White 1997, Huss, Jain & Steinmetz 1997, 1999, Thomas *et al.*, 1998). Recently, though, high resolution simulations of cluster formation in a CDM model, by Moore *et al.* (1998), yielded a core density profile $\rho(r) \propto r^{-1.4}$, shallower than r^{-2} , but steeper than the r^{-1} form preferred by NFW, consistent with the earlier high resolution work of Xu (1995). (For smaller mass halos, Kravtsov *et al.* (1998) find the core density profile to be shallower than the NFW form). It is important to understand these results as well on general theoretical grounds.

In a companion paper SCO99, we explore the possibility that a nested sequence of undigested cores in the center of a halo, which have survived the inhomogeneous collapse to form larger and larger objects, determine halo structure in the inner regions. For a flat universe with a power spectrum of density fluctuations $P(k) \propto k^n$, scaling arguments then suggest that the core density profile scales as, $\rho \propto r^{-\alpha}$ with $\alpha = \alpha_n = (9 + 3n)/(5 + n)$. But whether such a scaling law indeed obtains depends on the detailed dynamics.

Similarity solutions often provide a tractable, semi-analytic route to study time dependent dynamics in complicated physical systems. Fillmore and Goldreich (FG, 1984) and Bertschinger (B85, 1985) derived such solutions for describing the purely radial collapse of cold, collisionless matter in a perturbed Einstein-de Sitter universe. These solutions need to be generalised to incorporate tangential velocity dispersions, which as we see below, turn out to be crucial to understand density profiles shallower than $1/r^2$. Some general, analytical aspects of the similarity solutions incorporating tangential velocity dispersions are outlined in the companion paper SCO99. In the present paper, we consider these self-similar collapse solutions in greater detail, by deriving and solving numerically the scaled moment equations for such a collapse, including the effect of velocity dispersions.

In the next section we formulate the self-similar collapse problem and introduce a fluid approach for its solution, recapitulating the corresponding discussion in SCO99. In Section 3 we derive scaled moment equations describing the collapse and discuss their numerical solution. Specific numerical examples of self-similar collapse are given in Section 4. These solutions include the effect of halo velocity dispersions (both radial and tangential), and consider a range of spherically averaged initial density profiles. The final section discusses the results and presents our conclusions.

2. The self-similar solution

We summarize in this section, some of the properties of the similarity solution, that can be derived by analytic arguments. Although much of this section is mostly a recapitulation of Section

3 of SCO99, we include it here to make the present paper as self-contained as possible, and also to set the framework for the detailed numerical work which follows.

Consider the collapse of a single spherically symmetric density perturbation, in a flat background universe. Assume the initial density to be a power law in radius. We expect to describe the dynamics through a self-similar solution. FG and B85 looked at the self-similar evolution by following the self-similar particle trajectory. We adopt a different approach, by examining directly the evolution of the phase space density. During the course of this work we have learned that several authors (Padmanabhan 1994, unpublished notes; Padmanabhan 1996a, Chieze, Teyssier and Alimi 1997; Henriksen and Widrow 1997) have also adopted this approach to the purely radial self-similar collapse of FG and B85. We will emphasise and incorporate here also an additional aspect, the distinctive role of non-radial motions (velocity dispersions) in self-similar collapse.

The evolution of dark matter phase space density $f(\mathbf{r}, \mathbf{v}, t)$ is governed by the Vlasov Equation,

$$\frac{\partial f}{\partial t} + \mathbf{v} \cdot \frac{\partial f}{\partial \mathbf{r}} + \mathbf{a} \cdot \frac{\partial f}{\partial \mathbf{v}} = 0 \quad (1)$$

where \mathbf{r} and $\mathbf{v} = \dot{\mathbf{r}}$ are the proper co-ordinate and velocity of the particles respectively. Also the acceleration $\mathbf{a} = \dot{\mathbf{v}} = -\nabla\Phi$, with

$$\nabla^2\Phi = 4\pi G\rho = 4\pi G \int f d^3\mathbf{v} \quad (2)$$

By direct substitution, it is easy to verify that these equations admit self similar solutions of the form

$$f(\mathbf{r}, \mathbf{v}, t) = k_2 k_1^{-3} t^{-q-2p} F\left(\frac{\mathbf{r}}{k_1 t^p}, \frac{\mathbf{v}}{k_1 t^q}\right); \quad p = q + 1 \quad (3)$$

where k_1, k_2 are constants which we will fix to convenient values below. We have used proper co-ordinates here since the final equilibrium halo is most simply described in these co-ordinates. (The same solution in co-moving co-ordinates is given in Padmanabhan (1996a)). Defining a new set of co-ordinates $\mathbf{y} = \mathbf{r}/(k_1 t^p)$, $\mathbf{w} = \mathbf{v}/(k_1 t^q)$ and a scaled potential $\chi = k_1^{-2} t^{-2q} \Phi$, the scaled phase space density F satisfies

$$-(q + 2p)F - p\mathbf{y} \cdot \frac{\partial F}{\partial \mathbf{y}} - q\mathbf{w} \cdot \frac{\partial F}{\partial \mathbf{w}} + \mathbf{w} \cdot \frac{\partial F}{\partial \mathbf{y}} - \nabla_{\mathbf{y}}\chi \cdot \frac{\partial F}{\partial \mathbf{w}} = 0; \quad (4)$$

$$\nabla_{\mathbf{y}}^2 \chi = 4\pi G k_2 \int F d^3\mathbf{w}. \quad (5)$$

Consider the evolution of a spherically symmetric density perturbation, in a flat universe whose scale factor $a(t) \propto t^{2/3}$. For self similar evolution, the density is given by

$$\rho(r, t) = \int f d^3\mathbf{v} = k_2 t^{-2} \int F(y, \mathbf{w}) d^3\mathbf{w} \equiv k_2 t^{-2} \psi(y) \quad (6)$$

where we have defined $r = |\mathbf{r}|$, $y = |\mathbf{y}|$ and used the relation $p = q + 1$. For the flat universe, the background matter density evolves as $\rho_b(t) = 1/(6\pi G t^2)$. So the density contrast $\rho(r, t)/\rho_b(t) = \psi(y)$, where we take $k_2 = 1/(6\pi G)$.

2.1. Linear and non-linear limits

Let the initial excess density contrast averaged over a sphere of co-moving radius $x = r/a(t) \propto rt^{-2/3}$ be a power law $\bar{\delta}(x, t_i) \propto x^{-3\epsilon}$. Since ρ/ρ_b is a function of y alone, the $\bar{\delta}(x, t)$ will also be a function only of y . Note that, in the linear regime, the excess density contrast averaged over a *co-moving* sphere, grows as the scale factor $a(t)$. So one can write for the linear evolution of the spherical perturbation

$$\bar{\delta}(r, t) = \bar{\delta}_0 x^{-3\epsilon} t^{2/3} \propto \bar{\delta}_0 r^{-3\epsilon} t^{2/3+2\epsilon} \propto \bar{\delta}_0 y^{-3\epsilon} t^{-3\epsilon p+2/3+2\epsilon}, \quad (7)$$

where we have substituted $r \propto yt^p$. This can be a function of y alone, for a range of t in the linear regime iff $-3\epsilon p + 2/3 + 2\epsilon = 0$, which gives

$$p = \frac{2 + 6\epsilon}{9\epsilon} \quad (8)$$

We see that once the initial density profile is specified the exponents p, q of the self similar solution are completely determined.

Consider now what happens in the non-linear limit. The zeroth moment of the Vlasov equation gives

$$\frac{\partial \rho}{\partial t} + \nabla_{\mathbf{r}} \cdot (\rho \bar{\mathbf{v}}) = 0 \quad (9)$$

Here $\bar{\mathbf{v}} = \langle \mathbf{v} \rangle$ is the mean velocity. (Henceforth both $\langle \rangle$ or a bar over a variable denotes a normalised moment over f). In regions which have had a large amount of shell crossings, it seems plausible to demand that the halo particles have settled to nearly zero average infall velocity, that is $\bar{v}_r \equiv 0$. From (9), we then have $(\partial \rho / \partial t) = 0$, and therefore, in the non-linear regime,

$$\rho(r, t) = Q(r) = Q(yt^p) = \frac{1}{6\pi G t^2} \psi(y). \quad (10)$$

This functional equation has only power law solution, because of the power law dependences on t . Substituting $Q(r) = q_0 r^{-\alpha}$ into Eq. (10), and using $r \propto yt^p$, we obtain $y^{-\alpha} t^{-p\alpha} \propto t^{-2} D(y)$. This can only be satisfied for range of t in the non-linear regime provided $p\alpha = 2$. So, for an initial density profile with a power law slope 3ϵ , the power law slope of the density in the non-linear regime is given by,

$$\alpha = \frac{2}{p} = \frac{9\epsilon}{3\epsilon + 1}. \quad (11)$$

This result has been obtained by following the self similar particle trajectory, by B85 (for $\epsilon = 1$), and FG for $2/3 \leq \epsilon < 1$. We see that it can be simply obtained by just combining the self-similar solution f and the static core condition. (Obtaining the B85/FG result in this way has been independently noted by Padmanabhan (private communication, unpublished notes 1994)).

What should we choose for the value of ϵ ? For a power law $P(k) \propto k^n$, the fractional density contrast averaged over a co-moving sphere of radius x , is distributed as a Gaussian, with a variance $\propto x^{-(3+n)/2}$. This suggests a "typical" spherically averaged initial density law for a halo collapsing

around a randomly placed point of the form $\bar{\delta}(x, t_i) \propto x^{-(3+n)/2}$, or $3\epsilon = (3+n)/2$. Suppose we use this value of ϵ for the initial density profile of a halo. Then the halo density in the static core regions will be $\rho(r, t) \propto r^{-\alpha}$, where, substituting $3\epsilon = (3+n)/2$ in Eq. (11)

$$\alpha = \alpha_n = \frac{9 + 3n}{5 + n} \quad (12)$$

Remarkably, this is the same form that scaling laws suggest, for the core of a collapsed halo, assuming that the cores of sequence of sub-halos are left undigested, during the formation of the bigger halo (see SCO99). (In a paper which appeared during the course of this work, Syer & White (1998) motivate the same form, in the case when bigger halos form by purely merger of smaller halos). Note that for $n < 1$ the density law given by (12) is shallower than $1/r^2$.

FG also showed that a power law slope shallower than $1/r^2$, cannot obtain for purely radial collapse, And that while the above form for α should obtain for $2/3 \leq \epsilon < 1$, for $\epsilon < 2/3$, one goes to the limiting value $\alpha = 2$. However, this is only true for purely radial trajectories (cf. White and Zaritsky 1992; Sikvie, Tkachev and Wang 1997). We see below, by considering the higher moments of the Vlasov equation, that $\alpha < 2$ can only obtain if the system has non-radial velocity dispersions.

2.2. Jeans and Energy equations

Suppose we multiply the Vlasov equation by the components of \mathbf{v} and integrate over all \mathbf{v} . Assume there is no mean rotation to the halo, that is $\bar{v}_\theta = 0$ and $\bar{v}_\phi = 0$. Then we get

$$\frac{\partial(\rho\bar{v}_r)}{\partial t} + \frac{\partial(\rho\bar{v}_r^2)}{\partial r} + \frac{\rho}{r}(2\bar{v}_r^2 - \bar{v}_\theta^2 - \bar{v}_\phi^2) + \frac{GM(r)\rho}{r^2} = 0 \quad (13)$$

$$\bar{v}_\theta^2 = \bar{v}_\phi^2 \quad (14)$$

Here $M(r)$ is the mass contained in a sphere of radius r .

Let us consider again a static core with $\bar{v}_r \equiv 0$. The Jeans equation gives two equations for the three unknown velocity dispersions, even for a static core. To see if one can close the system SCO99 considered the second moments of the Vlasov equation (the energy equations). However these will involve the third moments, or the peculiar velocity skewness. Some form of closure hypothesis is needed in a fluid treatment of the Vlasov equation. For this we proceed as follows: One can firstly assume that initially the tangential velocities have zero skewness. Then in purely spherically symmetric evolution they would not develop any skewness, that is $\bar{v}_\theta^3 = \bar{v}_\phi^3 = \langle v_\theta v_\phi^2 \rangle = 0$ for all times. Also if the initial velocity ellipsoid had one of its principle axis pointing radially, we do not expect this axis to become misaligned in purely spherical evolution. This means we can assume $\langle v_r v_\theta^2 \rangle = \bar{v}_r \bar{v}_\theta^2$. Under these assumptions, and taking the static core condition $\bar{v}_r = 0$, we get, $(\partial(\rho\bar{v}_\theta^2)/\partial t) = 0$ or $\rho\bar{v}_\theta^2 = K(r)$ independent of t . For the self-similar

solution we then have

$$\rho \bar{v}_\theta^2 = K(r) = K(yt^p) = k_2 k_1^2 t^{4q-2p} \int w_\theta^2 F(y, \mathbf{w}) d^3 \mathbf{w} \quad (15)$$

Once again substituting a power law solution $K(r) = K_0 r^s$, to this functional equation, we get the constraint from matching power of t on both sides, $ps = 4q - 2p$. Using $p = q + 1$, we then get $s = 2 - 4/p = 2 - 2\alpha$, and so

$$\rho \bar{v}_\theta^2 = K_0 r^{2-2\alpha} \quad (16)$$

Integrating the radial momentum equation using Eq. (13), (14), (16) and using $\rho = q_0 r^{-\alpha}$, we have

$$\begin{aligned} \bar{v}_r^2 &= r^{2-\alpha} \left[\frac{K_0}{(2-\alpha)q_0} - \frac{4\pi G q_0}{2(2-\alpha)(3-\alpha)} \right] \\ &\equiv \frac{1}{(2-\alpha)} \left[\bar{v}_\theta^2(r) - \frac{GM(r)}{2r} \right]. \end{aligned} \quad (17)$$

Several important points are to be noted from the above equation¹. A crucial one is that, when $\alpha < 2$, the RHS of Eq. (17) can remain positive, provided one has a non zero tangential velocity dispersions. If one has a purely spherically symmetric collapse and zero tangential velocities, then the density law cannot become shallower than $\alpha = 2$ and maintain a static core with $\bar{v}_r = 0$. This agrees with FG. Infact for any $\alpha < 2$, one needs tangential velocity dispersions to be at least as large as $GM/2r$, comparable to the gravitational potential energy per unit mass. Further, one can see that to obtain static cores with $\alpha < 1$, the required tangential dispersions have to be necessarily larger than the radial velocity dispersions. Also note that for $\alpha < 2$, all the components of velocity dispersions decrease with decreasing radius, as suggested by the simple scaling arguments of SCO99.

For a static core \bar{v}_r^2 should be independent of t . However suppose we look at the the energy equation for the radial velocity dispersion,

$$\frac{\partial(\rho \bar{v}_r^2)}{\partial t} + \frac{1}{r^2} \frac{\partial(\rho r^2 \bar{v}_r^3)}{\partial r} - \frac{2\rho \langle v_r(v_\theta^2 + v_\phi^2) \rangle}{r} + 2\bar{v}_r \rho GM/r^2 = 0. \quad (18)$$

This shows that, even when $\bar{v}_r = 0$, a time independent radial velocity dispersion can only obtain if the radial velocity skewness $\langle (v_r - \bar{v}_r)^3 \rangle$ is also zero. In the core regions where large amounts of shell crossing has occurred, one can assume that a quasi "equilibrium" state obtains, whereby all odd moments of the distribution function, over $(\mathbf{v} - \bar{\mathbf{v}})$, may be neglected. Such a treatment will correspond to considering a fluid like limit to the Vlasov equation.

However, the radial skewness will become important near the radius, where infalling matter meets the outermost re-expanding shell of matter. This region will appear like a shock front in the

¹A constant of integration could have arisen in integrating the Jeans equation over radius; however this is excluded as, for a static core, arguments similar to deriving (15) and (16), give $\rho \bar{v}_r^2 \propto r^{2-2\alpha}$, for the self-similar solution.

fluid limit. A possible treatment of the full problem in the fluid approach to the Vlasov equation then suggests itself. This is to take the radial skewness to be zero both inside and outside a "shock or caustic" radius, whose location is to be determined as an eigenvalue, so as to match the inner core solution that we determine in this section with an outer spherical infall solution. One has to also match various quantities across this "shock", using jump conditions, derived from the equations themselves. To do this requires numerical solution of the self consistent set of moment equations derived from the scaled Vlasov equation (the main focus of this paper), to which we now turn.

3. Numerical solution of moment equations for self similar collapse

3.1. Moment equations

We write the scaled Vlasov equation (4) in spherical co-ordinates and take moments. Let us define $V = \bar{w}_r$, $\Pi = \langle (w_r - \bar{w}_r)^2 \rangle$ and $\Sigma = \bar{w}_\theta^2 = \bar{w}_\phi^2$. We also set the tangential velocity skewness to zero. As explained above, we take the radial skewness to be zero both inside and outside a "shock or caustic" radius. The shock location, say $y = y_s$ in scaled co-ordinates, will be determined as an eigenvalue, to the complete problem. So we set $\langle (w_r - \bar{w}_r)^3 \rangle = 0$ in the regions of interest, $y < y_s$ and $y > y_s$. The resulting moment equations can be further simplified with a little algebra and then can be written in the following more transparent form:

$$\frac{1}{y^2} \frac{d}{dy} [y^2 \psi V] - 2\psi - py \frac{d\psi}{dy} = 0 \quad (19)$$

$$(p-1)\psi V + \psi(V - py) \frac{dV}{dy} = -\frac{1}{y^2} \frac{d}{dy} [y^2 \psi \Pi] + \frac{2\psi \Sigma}{y} - \frac{\bar{M}\psi}{6\pi y^2} \quad (20)$$

$$(V - py) \frac{d}{dy} \left[\ln \left(\frac{\psi \Pi y^2}{(\psi y^2)^3} \right) \right] = 2p - 2 \quad (21)$$

$$(V - py) \frac{d}{dy} [\Sigma y^2] + (4p - 2)\Sigma y^2 = 0 \quad (22)$$

$$\frac{d\bar{M}}{dy} = 4\pi y^2 \psi \quad (23)$$

These equations have obvious meaning: Eq. (19) is the continuity equation for the scaled density, (20) the scaled Euler equation and (21) the scaled energy equation. Angular momentum conservation is reflected in Eq. (22) for Σ . It should be noted that the energy equation reflects the more general conservation P/λ^3 along fluid trajectories, where $\lambda = \rho r^2$ is an effective linear radial density and $P = \lambda \langle (v_r - \bar{v}_r)^2 \rangle$ is the effective radial pressure. Infact our system behaves like a monodimensional gas with an effective adiabatic index $\gamma = 3$, provided one takes the density to be the linear radial density λ , and defines the pressure P as above.

Both radial and tangential velocity dispersions are likely to be generated during the inhomogeneous collapse to form the halo. So it is natural take the initial, pre-collapse, velocity dispersions to be small. In the problem we are treating, of purely spherical collapse, the radial velocity dispersions will automatically be generated when spherically collapsing shells start to cross, that is where the radial skewness is important. In our fluid approach we will be replacing this region where radial skewness is important by a shock front. On the other hand, note that there are no source terms in the moment equations for the tangential velocity dispersions. Indeed in a purely spherically symmetric problem tangential velocities have to be necessarily introduced in an ad-hoc fashion. They are only non zero if present in the initial conditions.

White and Zaritsky (1992) introduced tangential velocities into their solutions by invoking a fictitious tangential force which act on particles in each spherical shell, until the shell turns around. Since in a general inhomogeneous collapse, one expects all the components of the velocity dispersion to be generated together, the shock gives an alternate natural location to introduce a tangential velocity dispersion, as well. We will do this here, for most of the numerical examples. Further in a non spherical, asymmetric collapse, the random velocities induced at the shock would be in general non-radial (cf. Ryden 1993), and the spherical models with both tangential and radial velocity dispersions introduced at the shock, may represent this in a rough way. (For comparison, we will also present a few examples in the next section, with the tangential velocity dispersion introduced at the turn around radius.) Studies of halo formation using cosmological N-body simulations, which are discussed in SCO99, can redress this deficiency of the spherical treatment.

The evolution of the region before shell crossings is determined by the spherical infall solution. At some initial time t_i , let the excess density contrast averaged over a sphere of proper initial radius r_i be $\bar{\delta}_i(r_i) = \delta_0(r_i/r_0)^{-3\epsilon}$. Then the shell initially at r_i will turnaround and collapse when it has expanded to a radius $r_i/\bar{\delta}_i(r_i)$ at a time $t = (3\pi/4)t_i/\bar{\delta}_i^{3/2}(r_i)$. The radius of a shell turning around at any time t is given by $r_t(t) = r_{0t}(t/t_{0t})^p$ where $p = (2 + 6\epsilon)/9\epsilon$ is as in Eq. (8). Also $r_{0t} = (r_0/\delta_0)$ and $t_{0t} = (3\pi/4)t_i/\delta_0^{3/2}$, are the turn-around radius and time of the shell initially at r_0 . Since $y = r/(k_1 t^p)$, a natural way of fixing the constant k_1 is by taking $k_1 t^p = r_t(t)$. We will do this in what follows. Then turn around occurs at the scaled co-ordinate $y = 1$.

A straightforward application of the spherical model (cf. Peebles 1980,, Padmanabhan and Subramanian 1992, Kumar, Padmanabhan, Subramanian 1995) then gives the solution of the moment equations, when $\Pi = \Sigma = 0$, in the region $y > y_s$. Expressed in a parametric form we have for $y > y_s$,

$$\begin{aligned}
 y &= \frac{r}{r_t(t)} = \frac{(1 - \cos \theta)\pi^p}{2(\theta - \sin \theta)^p}; & V(y) &= y \frac{\sin \theta(\theta - \sin \theta)}{(1 - \cos \theta)^2} \\
 \psi(y) &= \frac{9(\theta - \sin \theta)^2}{2(1 - \cos \theta)^3} \left[1 + 3\epsilon - \frac{9\epsilon \sin \theta(\theta - \sin \theta)}{2(1 - \cos \theta)^2} \right]^{-1}; & \bar{M}(y) &= \frac{4\pi y^3}{3} \frac{9(\theta - \sin \theta)^2}{2(1 - \cos \theta)^3} \quad (24)
 \end{aligned}$$

This goes over to the standard growing mode solution in the linear limit as $y \rightarrow \infty$.

3.2. Matching and boundary conditions

The equations (24) evaluated at $y = y_s$ gives the pre-shock boundary conditions to the moment equations. To match the spherical infall solution to the core solution for $y < y_s$ determined in the previous section, we have to specify the jump conditions across the shock at $y = y_s$. These conditions can be derived again in a straightforward manner from the moment equations. Suppose we denote the pre-shock values with subscript 1 and post shock values of all quantities with a subscript 2. Also we wish to consider the case when the pre-shock $\Pi_1 = 0$. Then the scaled jump conditions are given by

$$\psi_2 = 2\psi_1, \quad V_2 = py_s + \frac{1}{2}(V_1 - py_s), \quad \Pi_2 = \frac{(V_1 - py_s)^2}{4}, \quad \bar{M}_2 = \bar{M}_1 \quad (25)$$

In fact the jump conditions corresponds to taking $\gamma = 3$ in the usual fluid Rankine-Hugonot jump relations. These together with a non zero, *arbitrary* Σ_2 , gives the starting values for the numerical integration of the scaled moment equations (19) - (22) inward from the shock location $y = y_s$. The eigenvalue y_s is determined by requiring the solutions to satisfy the inner boundary conditions

$$V = M = 0, \quad y = 0 \quad (26)$$

To ensure the vanishing of the mass at $y = 0$, we have in fact integrated the scaled continuity equation and expressed the scaled mass in terms of the density and velocities. We have using (19) and (23)

$$\bar{M}(y) = \frac{4\pi y^2 \psi (V - py)}{2 - 3p} \quad (27)$$

The scaled density for all α and the scaled dispersions for $\alpha > 2$, are expected to be singular at the origin for the shocked infall solutions. So we scale out the expected asymptotic behaviour, at $y \rightarrow 0$, before numerical integration. If we are to obtain a nearly static core, we expect $V \rightarrow 0$ and $dV/dy \rightarrow 0$ as $y \rightarrow 0$. In this case, an analysis of the moment equation shows (see also section 2),

$$\psi(y) = y^{-\alpha} \tilde{\psi}(y), \quad \Sigma(y) = y^{2-\alpha} \tilde{\Sigma}(y), \quad \Pi(y) = y^{2-\alpha} \tilde{\Pi}(y) \quad (28)$$

where $\tilde{\psi}(y)$, $\tilde{\Sigma}(y)$ and $\tilde{\Pi}(y)$ are expected to tend towards a constant value as $y \rightarrow 0$. The exact asymptotic dependence of $V(y)$ of course has to be determined by the numerical solution.

The moment equations (19) - (22) are numerically integrated, after eliminating the scaled mass using (27) and transforming to the dependent variables defined in Eq. (28). We adapted a NAG library routine which integrates the differential equations using a Runge-Kutta-Merson method, and solves the boundary value problem with Newton iteration in a shooting and matching technique. For a given ϵ , and a sufficiently large Σ_2 (when $\alpha < 2$), a unique value of y_s is found to satisfy the inner boundary conditions of (26). The moment equations lead to two conservation laws which can be used to provide a check on the numerical integration. These can be derived by using Eq. (27) and the moment equations. We have

$$\frac{\tilde{\Sigma}(y)}{\tilde{M}^\kappa(y)} = \text{const}, \quad \kappa = \frac{4 - \alpha}{3 - \alpha} \quad (29)$$

representing angular momentum conservation, where $\bar{M}(y) = y^{3-\alpha}\tilde{M}(y)$. And

$$\frac{\tilde{\Pi}(y)\tilde{M}^\mu(y)}{\tilde{\psi}^2(y)} = \text{const}, \quad \mu = \frac{2-\alpha}{3-\alpha} \quad (30)$$

representing energy conservation. At each point these two integrals of motion were checked and had relative errors less than $10^{-8} - 10^{-9}$, as in B85. A possible additional constraint on a solution is the asymptotic condition given by Eq. (17), for an almost static core. In terms of the scaled variables, static core solutions satisfy the constraint

$$\tilde{\Pi}(0) = \frac{1}{(2-\alpha)} \left[\tilde{\Sigma}(0) - \frac{\tilde{\psi}(0)}{3(3-\alpha)} \right]. \quad (31)$$

The equations of course cannot be integrated in practice upto $y \equiv 0$, but only upto some small $y = y_m$ which is generally $\sim 10^{-2.5} - 10^{-4}$. So this constraint can be checked at this minimum y . Also, in practice, $V(y_m)$ is not expected to be identically zero (unlike $V(0)$), and so one has to set it to a very small but non-zero value to obtain converged solutions. In general for the solutions obtained here, $V(y_m) = V_m \sim -1.0 \times 10^{-6}$ to -1.0×10^{-3} and $V_m/y_m \ll 1$. And the constraint (31) is satisfied at a few percent level. Let us now discuss particular numerical examples.

4. Numerical examples

4.1. Collapse onto a localised, overdense perturbation, $\epsilon = 1$ case

First we look at self-similar spherical secondary infall onto an initially localised, overdense perturbation, by adopting $\epsilon = 1$ and $\Sigma_2 = 0$. This problem was solved by B85 and FG by examining the self similar particle trajectory. The parameters for the numerical solution obtained here with the fluid approach are summarized in Table 1. We give there the assumed parameters, the derived eigenvalue y_s and the value of the scaled dependent variables at y_s and at the minimum $y = y_m$. We find the eigenvalue $y_s = 0.4628$ for the above parameters. B85 solving the problem by looking at particle trajectories got the location of the outermost caustic as $y_s = 0.364$. The difference between the location of the shock as determined by this work and B85 could be because we have replaced a smooth transition region for the collisionless fluid, where velocity skewness is important, by a discontinuous shock. B85 found that the scaled density could be fitted asymptotically by a form $\psi(y) \approx 2.79y^{-9/4}$ when they adopted a minimum $y = y_m \sim 0.02$ for the particle trajectory. We can integrate our equations and get converged solutions satisfying the boundary conditions upto $y_m \sim 2 \times 10^{-4}$. We find that $\psi(y) = \tilde{\psi}y^{-9/4} \approx 3.1y^{-9/4}$ at y_m , while at $y \sim 2 \times 10^{-2}$ we find $\tilde{\psi} \approx 2.5$. These numbers bracket the asymptotic value of $\tilde{\psi} \sim 2.79$ obtained in B85. So there is reasonable agreement between our work and B85, given the differences in the value of y_m and the very different approaches.

In Figure 1 we plot $V(y)$, $\log(\psi(y))$, $\log(\Pi(y))$, against $\log(y)$ for this solution with $\epsilon = 1$, $\Sigma_2 = 0$. We can define the scaled rotational velocity $U(y) = [(GM(r)/r)/(r_t/t)^2]^{1/2}$. In Figure

1 we also show a plot of $\log(U^2)$ versus $\log(y)$. We see that the velocity, $V(y)$, smoothly tends to zero as $y \rightarrow 0$. V_m for this case was -4.0×10^{-5} . To compare the asymptotic dependence of the scaled density, with that predicted above for a static core, we also show in the $\log(\psi)$ vs $\log(y)$ plot, density laws $\psi(y) \propto y^{-\alpha}$, with $\alpha = 9\epsilon/(1 + 3\epsilon)$ predicted in section 2, (dashed line) and $\psi(y) \propto y^{-2}$ (dot-dashed-dot line). These are normalized to agree with $\psi(y)$ at the minimum y shown in the figure. We see from figure 2 that as $y \rightarrow 0$, the density does go over to $\psi(y) \propto y^{-\alpha} \propto y^{-9/4}$, as expected for a static core, with $\epsilon = 1$. Overall, we recover the results of B85 and FG reasonably well with our fluid approach to the problem.

4.2. $\epsilon < 2/3$ cases and the importance of tangential dispersions

We then considered solutions for initial density profiles shallower than r^{-2} , or $\epsilon < 2/3$. For such shallow density profiles, if the collapse were purely radial, FG showed that the final density profile approaches a $1/r^2$ form. We find, as expected, that the nature of the solutions in this case, depends on the ratio of tangential to radial velocity dispersions. We illustrate this by considering two values of this ratio, which bracket the expected behaviour.

In Figure 2 we show the solution for the case $\epsilon = 0.4$, $\tilde{\Sigma}_2 = \Sigma_2 y_s^{2-\alpha} = 0.94$. The detailed solution for this case is given in Table 2. For this solution, the value of $y_s = 0.4955$. We show both $\log(\Pi(y))$ (solid line) and $\log(\Sigma(y))$ (dashed line) in the same plot, so that they can be easily compared. From the figure or the table one sees that tangential velocity dispersions for this solutions are everywhere larger than the radial dispersions, by a factor ~ 1.3 . (Or $(\Sigma/\Pi)^{1/2} \sim 1.3$). For $\epsilon = 0.4$, and a static core, we expect the scaled variables, to have the asymptotic behaviour given in Eq. (28), with $\alpha = 18/11$. We see from comparing the solid and dashed lined, in the $\psi(y) - y$ plot of Figure 2, that the density rises as $\psi \propto y^{-\alpha} \propto y^{-18/11}$ to a very good approximation, throughout the core. Also the velocity dispersions and rotation velocities decrease with decreasing radius, as the analytic theory of Section 2 (or Eq.(28)) predicts. Indeed, from Table 2, we see that all the variables $\tilde{\psi}(y)$, $\tilde{\Sigma}(y)$ and $\tilde{\Pi}(y)$ tend to constant values as $y \rightarrow 0$ to an excellent approximation. This case illustrates that it is possible to obtain solutions for $\epsilon < 2/3$, which have $\alpha = 9\epsilon/(1 + 3\epsilon) < 2$, provided the tangential velocity dispersions are large enough.

To illustrate the effect of decreasing tangential velocity dispersions, we show in Figure 3, the properties of a solution with $\epsilon = 0.4$, $\tilde{\Sigma}_2 = 0.65$. The parameters for this solution, are given in Table 1. The location of the shock is at $y_s = 0.3797$. We could get converged solutions with $y_m = 4.6 \times 10^{-3}$, and with the velocity $V_m = -1.75 \times 10^{-3}$. The core regions are nearly static but not completely so. But the constraint given by Eq. (31) is satisfied at the 2% level. For this case the radial velocity dispersions are everywhere larger than the tangential dispersions, by a factor ~ 1.15 as $y \rightarrow 0$. One sees a large difference between this solution (Figure 3) and the one obtained for larger tangential velocity dispersion (Figure 2). First we see that when radial dispersion dominates, the density profile is closer to the $\psi \propto y^{-2}$ form than the $\psi \propto y^{-\alpha}$ form, although neither provides a good fit. Second the velocity dispersions are reasonably constant with

radius as $y \rightarrow 0$ limit, instead of decreasing with decreasing radius. The rotation velocity is also flatter.

We also considered smaller values of ϵ . Figure 4 gives a solution with $\epsilon = 1/6$, (corresponding to $\alpha = 1$ or $n = -2$ in α_n), and $\tilde{\Sigma}_2 = 2.2$ and some parameters for this solution are given in Table 1. The eigenvalue $y_s = 0.2584$ and $(\Sigma/\Pi)^{1/2} \sim 1.33$ in the core. Note that for $\alpha = 1$, the constraint equation (31) for a static core implies that $\tilde{\Sigma}(0) = \tilde{\Pi}(0) + \tilde{\psi}(0)/6$. So $\tilde{\Sigma}(0)/\tilde{\Pi}(0) > 1$ for any solution with a static core. The density profile shows a reasonable correspondence with the asymptotic behaviour expected taking $\alpha = 1$; $\psi(y) \propto y^{-1}$. The velocity dispersions and the rotation velocity also decrease with decreasing y , but do so a little less rapidly compared to the predicted $\Sigma \propto \Pi \propto U^2 \propto y$ form.

In general, we find that, for smaller values of $\epsilon \leq 1/6$ (or $\alpha \leq 1$), while it possible to find static core solutions for a sufficiently large Σ/Π ratio, it becomes increasingly difficult to do so (obtaining a small enough V_m/y_m ratio) as one lowers the ratio of Σ/Π , to even slightly smaller values. We considered for example a case with $\epsilon = 1/6$, $\tilde{\Sigma}_2 = 2$. This turns out to have $\Sigma/\Pi \sim 1$, but we found that we could only decrease V_m/y_m to a value of order unity and get a solution. We get $V_m \sim 1.5 \times 10^{-2}$ and $dV/dy \sim 0.06$ at y_m ; so even though the core is not strictly static, the LHS of the scaled Euler equation (20) is much smaller than each of the individual force terms. These nearly cancel each other making the the core quasi-static. We give a plot of all the variables for this solution in Figure 5, and a summary of some parameters in Table 1. We see that the shape of the density profile for this solution is mid-way between the $r^{-\alpha} \propto r^{-1}$ form and r^{-2} form. The velocity dispersions are decreasing with radius but not as rapidly as predicted for a truly static core.

At this stage it is worthwhile to note the following: Recall that the static core condition used to derive the asymptotic scaling properties of the density and velocity dispersions, involves assuming not only $\bar{v}_r(0) = 0$ (the boundary condition adopted above), but also that the radial velocity vanishes for a range of radii near the origin. This situation can strictly obtain only if particles with a given turn around radius have a *minimum* radius of approach to the centre; so that the core at any radius r is evacuated of particles having turn around radii larger than say, $R_t(r)$. Such an "evacuated" core will inturn obtain only if the distribution of angular momentum has a "hole" near the origin of (v_θ, v_ϕ) plane. Such an angular momentum distribution is indeed assumed (and relevant) in the work of White and Zaritsky (1992). However, in the present work we are making the statistical assumption that the distribution of tangential velocities is well described by its second moment (viz. the tangential dispersion), thereby excluding distribution functions, which have a hole. This assumption is quite reasonable for halo cores with are forming by a general inhomogeneous collapse. However, in this case, for any shell of particles which pass the caustic at some epoch, there are always some particles with sufficiently small angular momentum, that can approach close to the halo core. So the halo core will not be strictly static, a feature which will be more and more noticeable, as one decreases tangential velocity dispersions relative to the radial dispersions. This may account for our result that (for $\epsilon < 2/3$), as one decreases Σ/Π , the density

profile is steeper than the $\psi \propto y^{-\alpha}$ form expected for a strictly static core.

Finally, for the sake of comparison, we have also looked at numerical examples where the tangential velocity dispersions are introduced at the 'turn around' radius (taken to be approximately at $y = 1$) rather than at the shock. In this case one has to solve the moment equations numerically, both outside and inside the shock radius, match the solutions across the shock, using the shock jump conditions (cf. Eq. (25) when $\Pi_1 = 0$), and find the shock location as an eigenvalue to satisfy the boundary conditions in Eq. (26). Figures 6 and 7 give two examples with $\epsilon = 0.4$, adopting $\tilde{\Pi}(1) = 0$ and $\tilde{\Sigma}(1) = 0.25$ and $\tilde{\Sigma}(1) = 0.30$, respectively. The parameters of these solutions are given in Table 1. When $\tilde{\Sigma}(1) = 0.25$, the force due to the tangential velocity dispersion at turn around is $\sim 13.5\%$ of the radial gravitational force. These examples show very similar behaviour to the $\epsilon = 0.4$ solutions discussed above (Figures 2 and 3), where the tangential velocities are introduced at the shock. For example, the solution shown in Figure 6, has $\Sigma/\Pi \sim 1$ in the core. The corresponding density profile is shallower than y^{-2} but steeper than the $y^{-\alpha}$ form, reflecting the fact that only a partial memory of the initial profile is retained by self-similar evolution in this case.

The numerical results of this section shows the importance of tangential velocity dispersions, in deciding whether the self similar solution, with an initial density profile shallower than $1/r^2$ ($\epsilon < 2/3$) retains a memory of this initial profile or whether the density profile tends to a universal $1/r^2$ form. The set of solutions we have given show that for a large enough $\Sigma/\Pi > 1$, the the core density profile is indeed close to the form $\rho \propto r^{-\alpha}$, with $\alpha = 9\epsilon/(1 + 3\epsilon)$. For $\Sigma/\Pi \sim 1$, some memory of the initial density profile is always retained; the density profile has an asymptotic form $\rho \propto r^{-\bar{\alpha}}$, with $\alpha < \bar{\alpha} < 2$. When $\Sigma/\Pi \ll 1$, the density profile goes over to the $1/r^2$ form derived by FG. Also for shallow initial density profiles with $\alpha \leq 1$, one must necessarily have a tangential dispersion larger than radial dispersion to get a static core region, retaining the memory of the initial density profile.

5. Discussion and Conclusions

We have explored here the dynamical restrictions on the structure of dark matter halos through a study of cosmological self-similar gravitational collapse solutions, adopting a fluid approach to the collisionless dynamics of dark matter. In a companion paper (SCO99) we consider the possibility that a nested sequence of undigested cores in the center of a halo, which have survived the inhomogeneous collapse to form larger and larger objects, determine halo structure in the inner regions. For a flat universe with $P(k) \propto k^n$, scaling arguments then suggest that the core density profile scales as, $\rho \propto r^{-\alpha}$ with $\alpha = \alpha_n = (9 + 3n)/(5 + n)$. However, such arguments do not tell us how and in fact whether this form will be realized dynamically. The similarity solutions worked out in some detail here, allows us to examine this dynamical issue, in a simple tractable manner.

The problem of spherical self similar collapse, has often been solved by following particle trajectories. We adopted here and in SCO99 another approach, examining directly the evolution of the moments of the phase space density. For a purely radial collapse, with the initial density profile $\propto r^{-3\epsilon}$, and steeper than r^{-2} , we recover, by demanding that the core be static, the asymptotic form of the non-linear density profile: $\rho \propto r^{-\alpha} \propto r^{-9\epsilon/(1+3\epsilon)}$ (see also Padmanabhan 1996b). For initial density profiles shallower than $1/r^2$, with $\epsilon < 2/3$, we showed that, a static core with a non-linear density profile, with $\alpha = 9\epsilon/(1 + 3\epsilon)$, is possible, only if the core has sufficiently large tangential velocity dispersions. Infact, one needs $\bar{v}_\theta^2 > GM/2r$. Also if a static core has to have a cuspy density profile shallower than $1/r$, (with $\alpha < 1$), one requires $\bar{v}_\theta^2 > \bar{v}_r^2$. Note that when $3\epsilon = (3 + n)/2$ (as would be relevant for collapse around a typical point in the universe), $\alpha = \alpha_n = (9 + 3n)/(5 + n)$.

The consequences of introducing non radial velocity dispersions, in this approach, can only be examined in detail, by adopting a closure approximation. In spherical collapse, the skewness of the tangential velocities can be assumed to be zero, in the core regions. In fact, in regions where large amounts of shell crossing has occurred, one can assume that a quasi "equilibrium" state obtains, whereby all odd moments of the distribution function, over $(\mathbf{v} - \bar{\mathbf{v}})$, may be neglected. The radial peculiar velocity is then also expected to have negligible skewness, in the core regions. However, the radial peculiar velocity will necessarily have a non-zero skewness (non zero third moment) near a caustic radius, where collapsing dark matter particles meet the outermost shell of re-expanding matter. To take this into account we introduce a fluid approach. In this approach, the effect of peculiar velocity skewness is neglected in all regions except at location of the caustic, which we call the shock. In the particle picture the shock is where a single stream flow becomes a muti stream flow. In the fluid picture it is a where some of the average infall velocity, is converted to velocity dispersion. The location of the caustic, y_s , in scaled co ordinates, is found as an eigenvalue, to the boundary value problem of matching the single stream collapse solution with a core solution, adopting $V = M = 0$ as the boundary condition at $y = 0$.

In spherical collapse tangential velocities are only non zero if they are present in the initial condition. The shock or the turn around radius, provide a natural location for introducing tangential dispersions, into the initial conditions. Our treatment here assumes that the distribution of tangential velocities is well described by just its second moment, consistent with the statistical assumptions of a quasi-relaxed core. The results of the numerical integration of the moment equations, are summarized in Table 1 and are graphically displayed in Figures 1-7. The details of one particular solution is also given in Table 2.

These examples largely bear out the expectations of section 2. First we recover quite well, using the fluid approach, the the asymptotic form of the non-linear density profile, for the $\epsilon = 1$ case, which B85/FG got by solving for the self-similar particle trajectory. Second our solutions show the importance of tangential velocity dispersions, in deciding the nature of the core density profile, when $\epsilon < 2/3$. In the spherical self similar collapse solutions with $\epsilon < 2/3$, for a large enough $\Sigma/\Pi > 1$, one gets $\rho \propto r^{-\alpha}$, with $\alpha = 9\epsilon/(1 + 3\epsilon)$. For $\Sigma/\Pi \sim 1$, some memory of the

initial density profile is always retained; one gets $\rho \propto r^{-\alpha}$, with $\alpha < \bar{\alpha} < 2$. When $\Sigma/\Pi \ll 1$, the density profile goes over to the $1/r^2$ form derived by FG for radial collapse. Also $\alpha < 1$, requires $\Sigma/\Pi \gg 1$, to get a static core region. So if in halo cores tangential velocities are constrained to be smaller than radial velocity dispersions, then a cuspy core density profile shallower than $1/r$ cannot obtain, purely by self-similar evolution.

The results of this work and SCO99, illustrate the importance of dynamical considerations and hint at features which are likely to obtain in more realistic collapse. If newly collapsing material is constrained to mostly contribute to the density at larger and larger radii, then memory of initial conditions can be retained. The solutions, with $\alpha > 2$ (Figure 1), or with $\alpha < 2$ but a large enough tangential dispersion (Figures 2 and 4), illustrate this possibility. However when newly collapsing material is able to occupy similar regions as the matter which collapsed earlier, the core density profile will only partially reflect a memory of the initial conditions. The solutions in Section 4 with $\alpha < 2$ and $\Sigma/\Pi \sim 1$ (Figures 3, 5 and 6) illustrates this feature.

In SCO99 we have also adopted a complimentary approach, of looking at halo properties in numerical simulations of structure formation models having $n = -2, -1$ and 0 . We find that the core density profiles of dark matter halos show a large scatter in their properties, but do nevertheless appear to reflect a memory of the initial power spectrum (please see SCO99 for details). The fluid approach adopted here and in SCO99 suggests new ways of exploring non linear dynamics. Perhaps one can extend analytic approximations like the Zeldovich approximation, valid in a single stream flow, to the multi streaming regime, by replacing multistreaming regions by regions with velocity dispersions, generated by the Zeldovich type caustics. The fluid approach could also be useful to study possible closures of the BBJKY hierarchy. Further one needs to extend the self-similar solutions to incorporate a baryonic component; the gas necessarily has an isotropic velocity dispersion, and so will have a different dynamical evolution compared to the dark matter. We hope to study some of these issues in the future.

KS thanks Jerry Ostriker and Renyue Cen for an enjoyable collaboration which led to this paper. This work was begun when KS visited the Princeton University Observatory, during Sept-Nov 1996. Partial travel support to Princeton came from IAU Commission 38. Some of the work was done at the University of Sussex where KS was supported by a PPARC Visiting Fellowship. He thanks John Barrow, Jerry Ostriker, Ed Turner, the other Princeton and Sussex astronomers for warm hospitality. T. Padmanabhan is thanked for critical comments on an earlier version of this work. KS also thanks Ben Moore, Bepi Tormen, Ravi Sheth, Dave Syer and Simon White for several helpful discussions.

REFERENCES

- Bertschinger, E. 1985, ApJS, 58, 39.
- Binney, J., and Tremaine, S., 1987, Galactic Dynamics, Princeton University Press.
- Cole, S. M., and Lacey, C., 1996, MNRAS, 281, 716.
- Chieze, J-P, Teyssier, R., and Alimi, J-M, 1997, ApJ, 484, 40.
- Fillmore, J. A., and Goldreich, P. 1984, ApJ, 281, 1.
- Henriksen, R. N., and Widrow, L. M., 1997, Phys. Rev. Lett., 78, 3426.
- Huss, A., Jain, B., and Steinmetz, M. 1997, preprint (astro-ph/9703014)
- Huss, A., Jain, B., and Steinmetz, M. 1999, ApJ, 517, 64.
- Kravtsov, A. V., Klypin, A. A., Bullock, J. S., and Primack, J. R., 1998, ApJ, 502, 48.
- Kumar, A., Padmanabhan, T., and Subramanian, K. 1995, MNRAS, 272, 544.
- Moore, B., Governato, F., Quinn, T., Stadel, J., and Lake, G. 1998, ApJL, 499, L5.
- Moore, B., Quinn, T., Governato, F., Stadel, J., and Lake, G. 1999, preprint (astro-ph/9903164).
- Navarro, J. F., Frenk, C. S., and White, S. D. M. 1995, MNRAS, 275, 720.
- Navarro, J. F., Frenk, C. S., and White, S. D. M. 1996, ApJ, 462, 563.
- Navarro, J. F., Frenk, C. S., and White, S. D. M. 1997, ApJ, 490, 493.
- Padmanabhan, T. 1993, Structure formation in the universe, Cambridge University Press.
- Padmanabhan, T. 1996a, Cosmology and astrophysics through problems, Cambridge University press.
- Padmanabhan, T. 1996b, MNRAS, 278, L29.
- Padmanabhan, T. and Subramanian, K. 1992, Bull. Astr. Soc. Ind., 20, 1.
- Peebles, P. J. E., 1980, The Large Scale Structure of the Universe, Princeton University Press.
- Ryden, B., 1993, ApJ, 418, 4.
- Sikvie, P., Tkachev, I. I., and Wang, Y. 1997, Phys. Rev. D, 56, 1863.
- Subramanian, K., Cen, R., and Ostriker, J. P., 1999, ApJ(submitted) (SCO99).
- Syer, D., and White, S. D. M., 1998, MNRAS, 293, 337.

Thomas, P. A., *et al.*, 1998, MNRAS, 296, 1061.

Tormen, G., Bouchet, F. R., and White, S. D. M. 1997, MNRAS, 286, 865.

White, S. D. M., and Zaritsky. 1992, ApJ, 394, 1.

Xu, G. 1995, Phd Thesis, Princeton University.

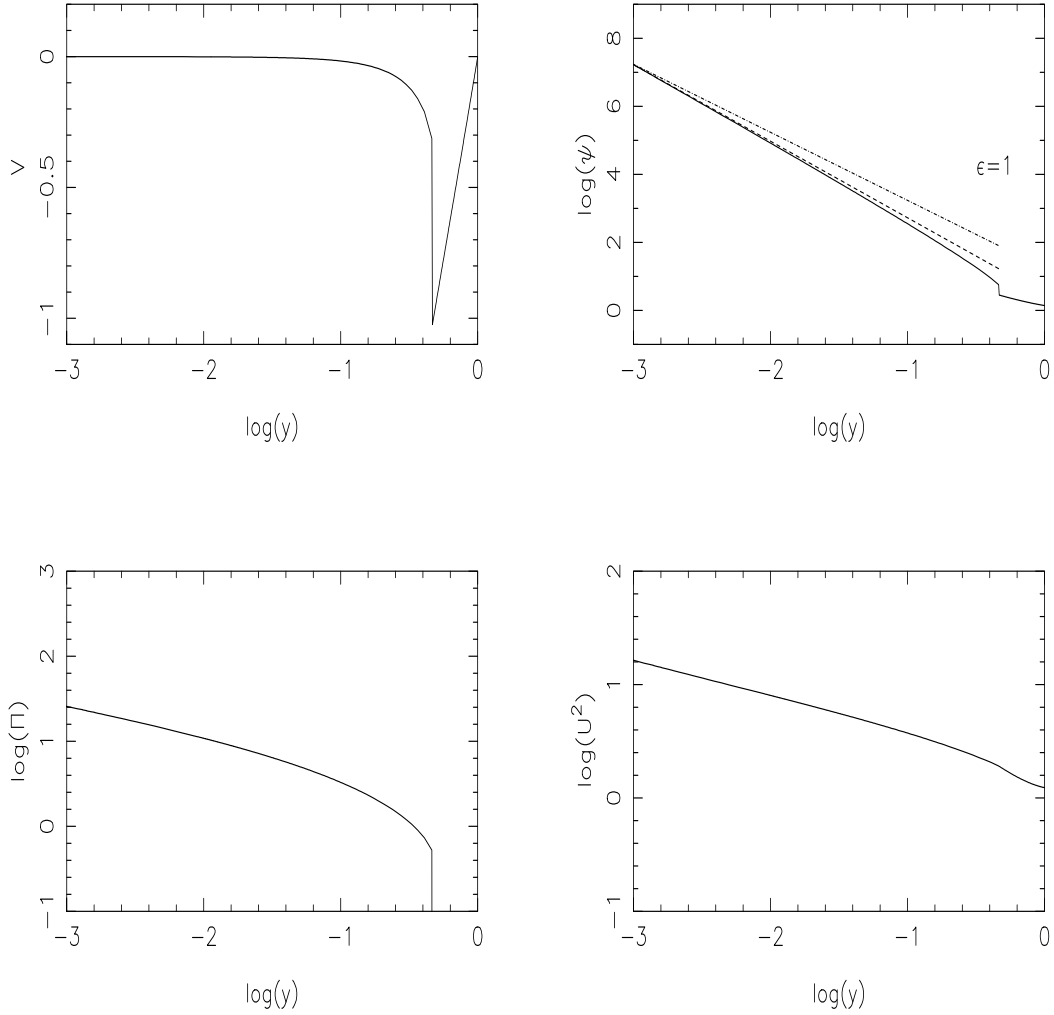


Fig. 1.— Self similar collapse solution for $\epsilon = 1$ case of B85/FG. The velocity V , scaled density ψ (solid line in the upper right plot), radial velocity dispersion squared Π , and circular velocity squared U^2 are plotted against the scaled radius y . The pre shock spherical infall solution is also shown. In the ψ - y plot we also show for comparison the density laws $\psi \propto r^{-\alpha}$ (dashed line) with $\alpha = 9\epsilon/(1 + 3\epsilon)$ and $\psi \propto r^{-2}$ (dashed -dotted line).

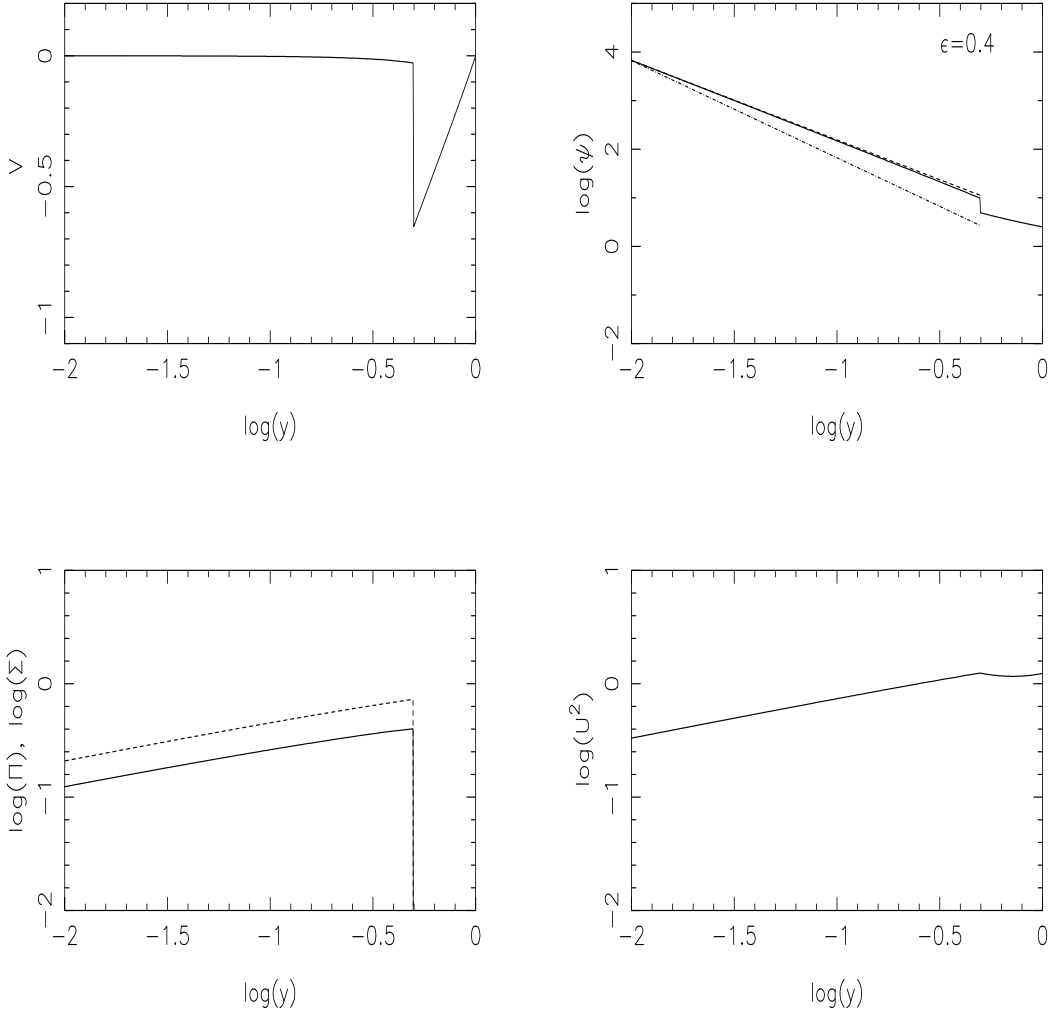


Fig. 2.— Self similar collapse solution for $\epsilon = 0.4$, $\tilde{\Sigma}_2 = 0.94$. The velocity V , scaled density ψ (solid line in the upper right plot), radial velocity dispersion squared Π (solid line in the lower left plot), tangential velocity dispersion squared Σ (dashed line in the lower left plot) and circular velocity squared U^2 are plotted against the scaled radius y . The pre shock spherical infall solution is also shown. In the ψ - y plot we also show for comparison the density laws $\psi \propto r^{-\alpha}$ (dashed line) with $\alpha = 9\epsilon/(1 + 3\epsilon)$ and $\psi \propto r^{-2}$ (dashed -dotted line).

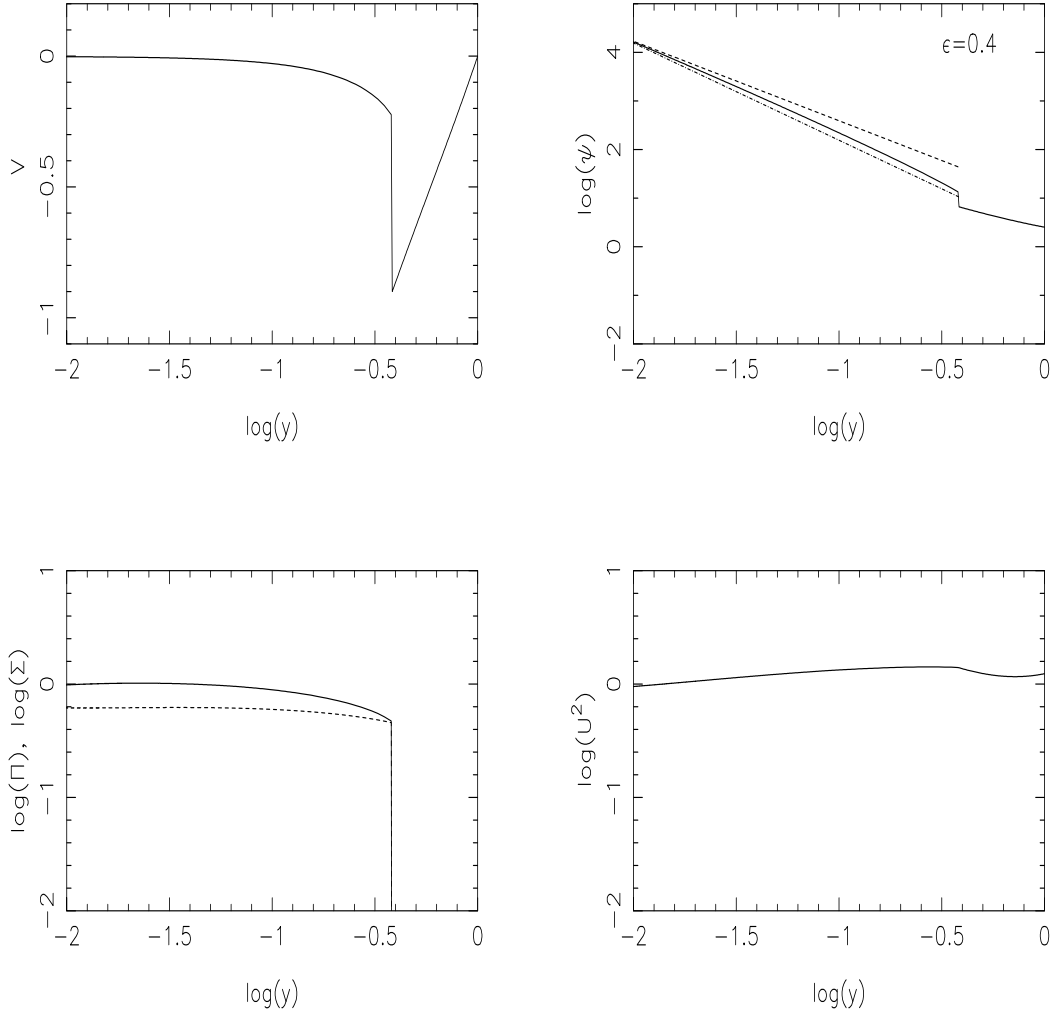


Fig. 3.— Self similar collapse solution for $\epsilon = 0.4$, $\tilde{\Sigma}_2 = 0.65$. The various quantities shown are same as in Fig. 2.

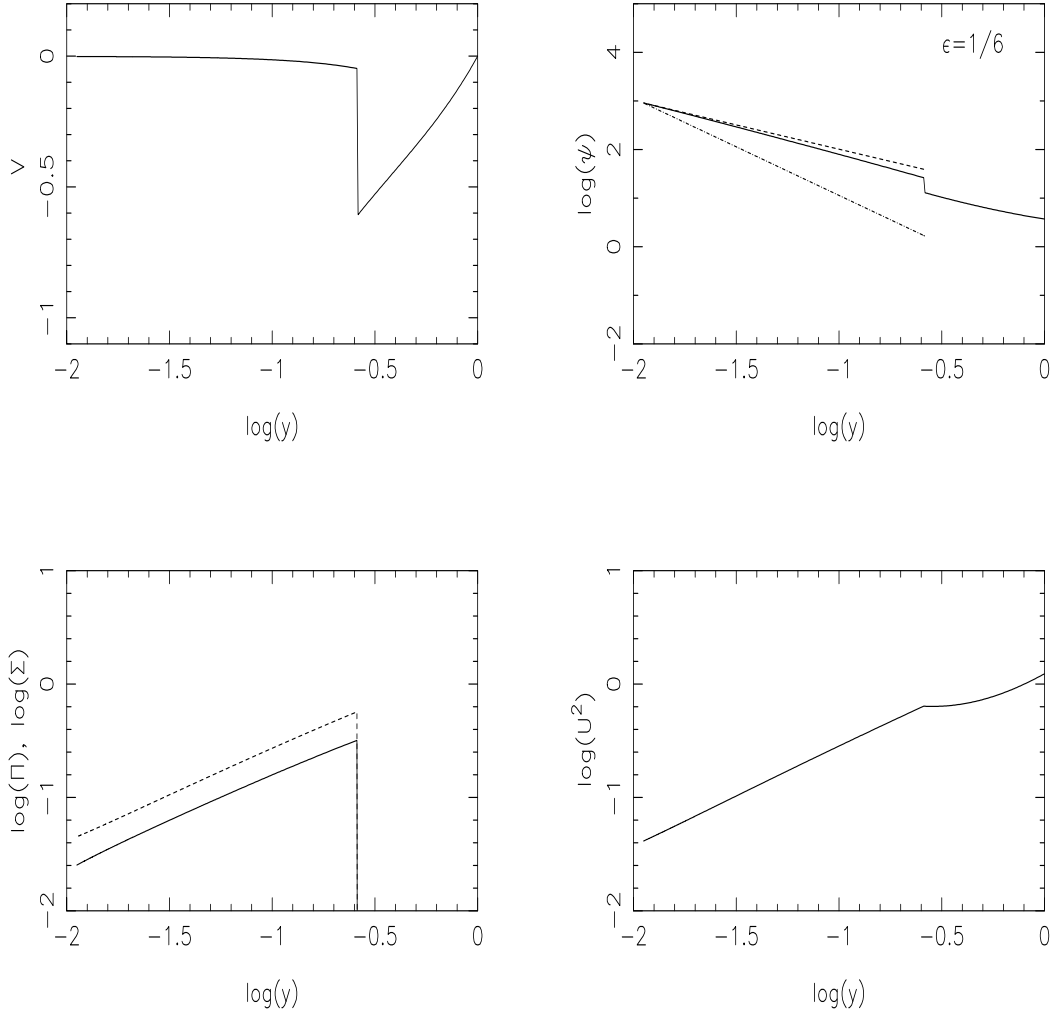


Fig. 4.— Self similar collapse solution for $\epsilon = 1/6$, $\tilde{\Sigma}_2 = 2.2$. The various quantities shown are same as in Fig. 2.

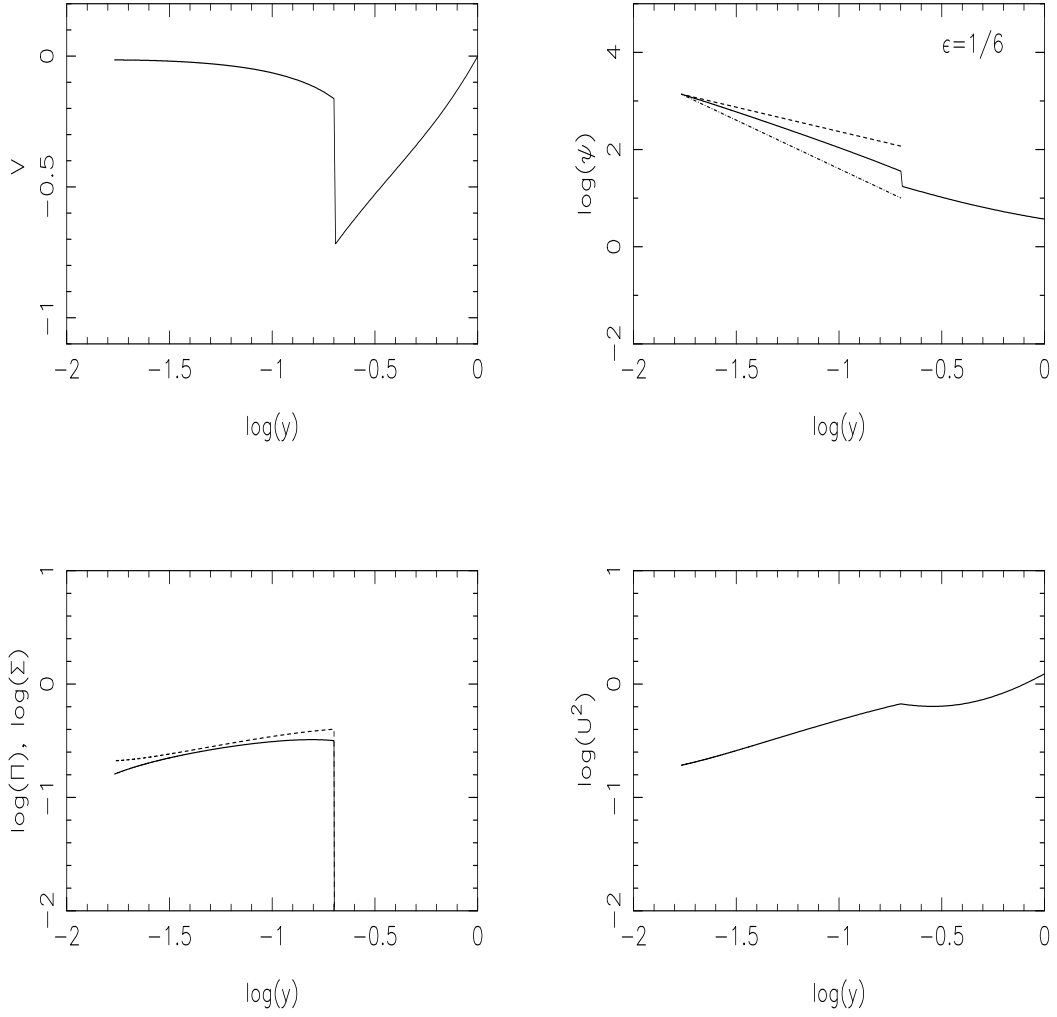


Fig. 5.— Self similar collapse solution for $\epsilon = 1/6$, $\tilde{\Sigma}_2 = 2.0$. The various quantities shown are same as in Fig. 2.

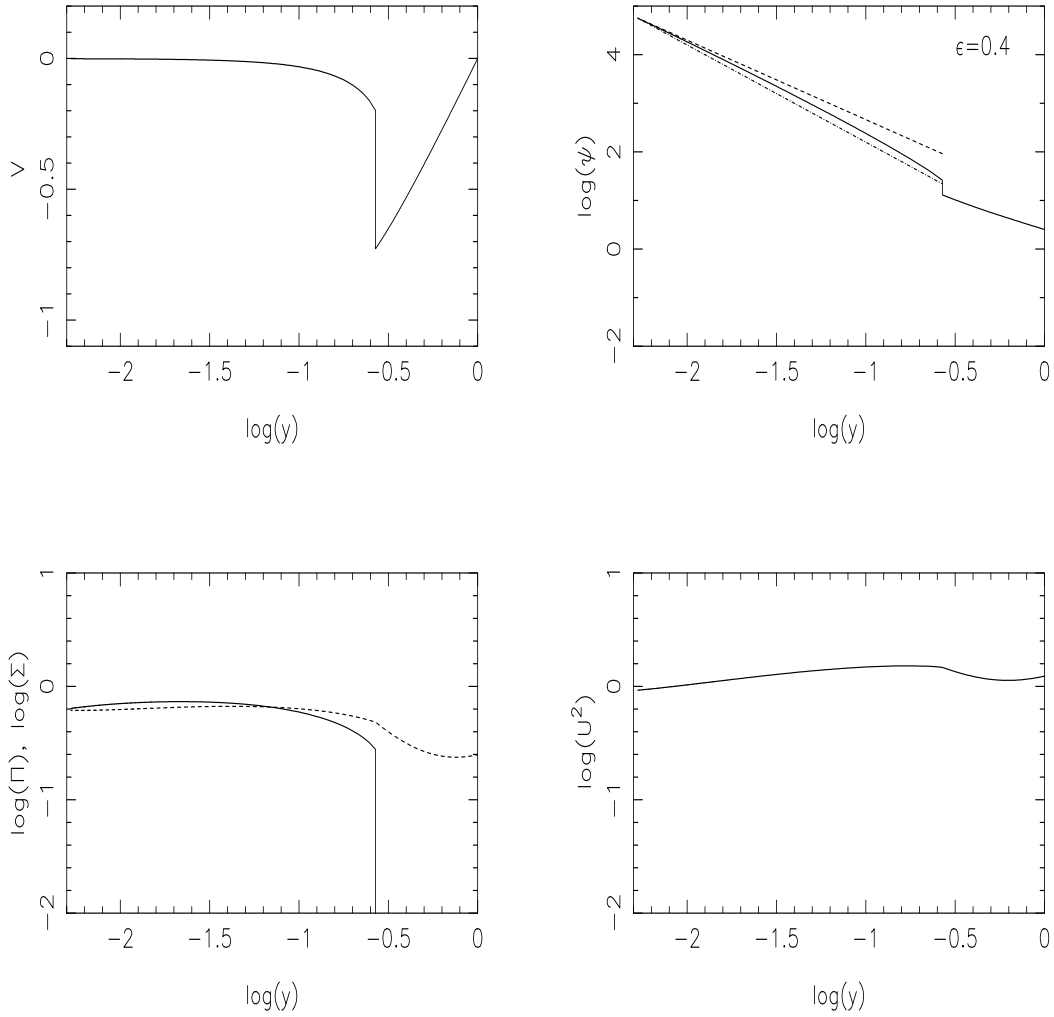


Fig. 6.— Self similar collapse solution for $\epsilon = 0.4$, $\tilde{\Sigma}_2(1) = 0.25$, $\tilde{\Pi}(1) = 0$. Here the tangential velocity dispersions have been introduced at the turn around radius corresponding to $y = 1$. The force due to the tangential velocity dispersion at turn around is 13.5% of the radial gravitational force. The various quantities shown are same as in Fig. 2.

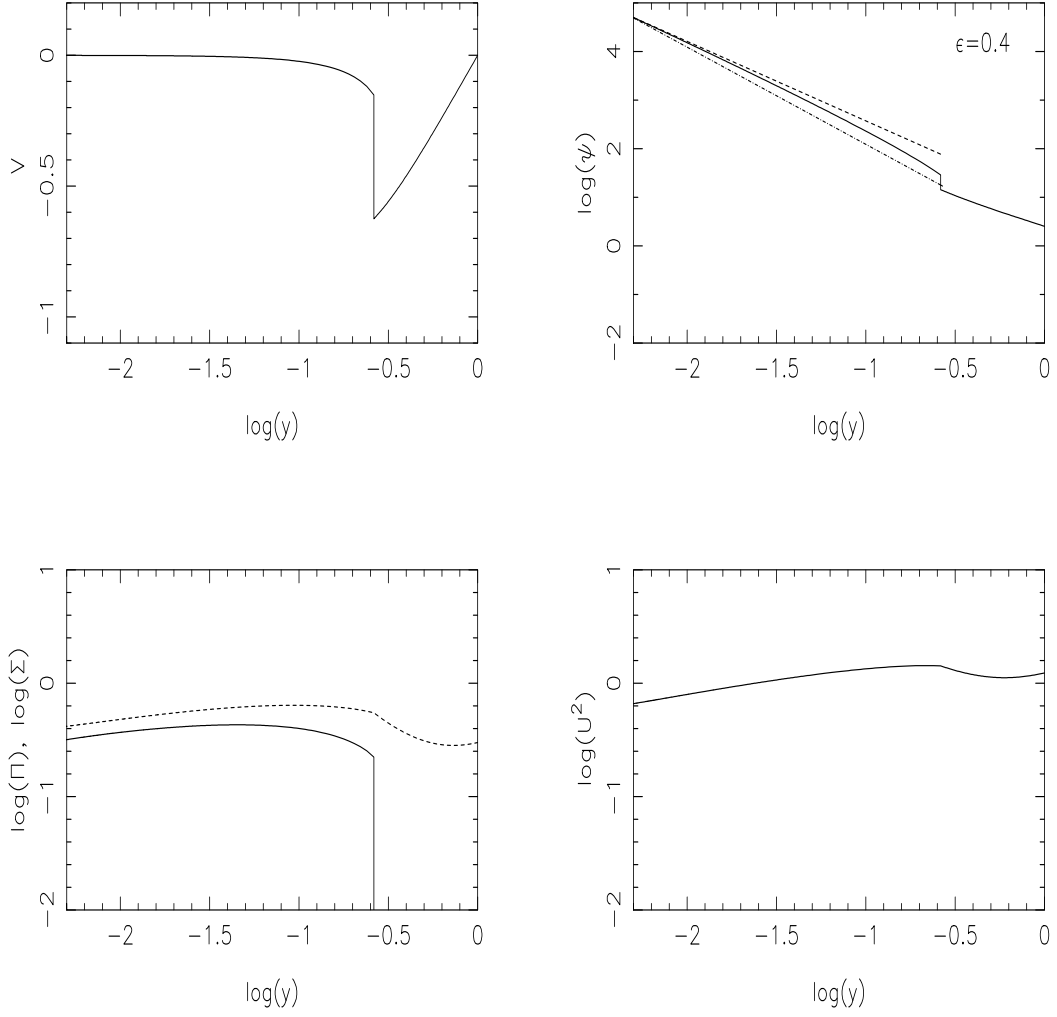


Fig. 7.— Self similar collapse solution for $\epsilon = 0.4$, $\tilde{\Sigma}_2(1) = 0.30$, $\tilde{\Pi}(1) = 0$. The tangential velocity dispersions have been introduced at the turn around radius corresponding to $y = 1$. The various quantities shown are same as in Fig. 2.

Table 1. The parameters of the self similar solutions

ϵ	$\tilde{\Sigma}_2$	y_s	V_2	$\tilde{\psi}_2$	$\tilde{\Sigma}_2$	$\tilde{\Pi}_2$	y_m	V_m	$\tilde{\psi}(y_m)$	$\tilde{\Sigma}(y_m)$	$\tilde{\Pi}(y_m)$
1	0	0.4628	-0.313	1.009	0	0.433	1.7E-4	-4.0E-5	3.139	0	5.464
0.4	0.94	0.4955	-0.0273	3.141	0.94	0.517	2.86E-3	-1.0E-6	3.641	1.126	0.676
0.4	0.65	0.3797	-0.223	2.750	0.65	0.672	4.62E-3	-1.75E-3	9.691	4.661	6.162
1/6	2.2	0.2584	-0.0473	6.785	2.2	1.232	1.12E-2	-2.0E-3	10.16	4.021	2.261
1/6	2.0	0.1999	-0.163	7.140	2.0	1.584	1.56E-2	-1.5E-2	24.17	13.45	9.615
	$\tilde{\Sigma}(1)$										
0.4	0.25	0.2684	-0.1995	3.024	0.78	0.449	5.2E-3	-1.27E-3	10.67	4.180	4.318
0.4	0.30	0.2622	-0.1521	3.210	0.89	0.363	4.5E-3	-4.5E-4	8.657	2.909	2.203

Table 2. The self similar solutions with $\epsilon = 0.4$, $\tilde{\Sigma}_2 = 0.94$

y	$V(y)$	$\tilde{\psi}(y)$	$\tilde{\Sigma}(y)$	$\tilde{\Pi}(y)$	$\tilde{M}(y)$
0.4955	-2.725E-02	3.141	0.940	0.517	30.24
0.4562	-2.353E-02	3.164	0.948	0.524	30.39
0.4226	-2.064E-02	3.184	0.955	0.530	30.51
0.3937	-1.832E-02	3.201	0.961	0.535	30.62
0.3684	-1.643E-02	3.217	0.966	0.540	30.72
0.3265	-1.352E-02	3.243	0.975	0.548	30.90
0.2932	-1.141E-02	3.264	0.983	0.555	31.04
0.2660	-9.811E-03	3.283	0.990	0.560	31.16
0.2336	-8.036E-03	3.306	0.999	0.567	31.32
0.2009	-6.398E-03	3.331	1.008	0.575	31.49
0.1710	-5.027E-03	3.355	1.018	0.583	31.66
0.1415	-3.798E-03	3.381	1.028	0.591	31.85
0.1113	-2.671E-03	3.412	1.040	0.601	32.06
0.0802	-1.658E-03	3.448	1.054	0.613	32.32
0.0506	-8.514E-04	3.492	1.072	0.626	32.62
0.0201	-2.262E-04	3.558	1.098	0.648	33.09
0.0100	-8.091E-05	3.593	1.113	0.660	33.33
0.0080	-5.759E-05	3.603	1.116	0.663	33.39
0.0050	-2.493E-05	3.621	1.122	0.669	33.50
0.0040	-1.384E-05	3.629	1.124	0.672	33.54
0.0032	-4.482E-06	3.637	1.126	0.675	33.56
0.0029	-1.000E-06	3.641	1.126	0.676	33.56